J Mater Sci (2016) 51:3146–3154
DOI 10.1007/s10853-015-9624-6

Preparation of mesoporous silicoaluminophosphate using ammonium hydroxide as the base and its catalytic application in the *trans*-alkylation of aromatics

Arvind Kumar Singh[1] · Rekha Yadav[1] · Ayyamperumal Sakthivel[1]

Received: 18 August 2015 / Accepted: 25 November 2015 / Published online: 10 December 2015

Abstract Hierarchical mesoporous silicoaluminophosphate (M-S-34-N) was assembled for the first time in the presence of ammonium hydroxide as the base. The resulting materials were subsequently stabilized via vapor-phase treatment in presence of tetraethylorthosilicate (TEOS). N_2 sorption analysis and pyridine desorption studies revealed that materials possess uniform mesoporous channel with high surface area, large pore volume, and strong Lewis acidity, respectively. The local environment of aluminum and silicon were followed with solid-state ^{27}Al, and ^{29}Si MAS NMR spectral studies, which indicates their successful framework incorporation. The strong acidity present on the resultant M-S-34-N-VPT facilitates for liquid-phase *trans*-alkylation of naphthalene using 1,3-diisopropylbenzene.

Introduction

The tailored syntheses of open framework materials with desired molecular sieve architectures have shown vast applications in the field of catalysis, adsorption, ion exchange, and support [1–5]. The synthesis and improving structural properties of such framework materials have gained considerable attention in recent years [1–5]. Numerous studies have been reported on silicate-based molecular sieves and been extensively studied in several catalytic studies [4–8]. On the other hand, development of such a hybrid-hierarchical mesoporous aluminophosphate (APO)-based materials with different pore architectures, variable active centers, and improved catalytic activities has become an active area in materials research [9–12]. Such mesoporous materials overcome the pore constraints, diffusion limitation, and remote active site accessibility of their microporous counterparts. In contrast to mesoporous silicates, synthetic strategies for mesoporous APO materials involve the synchronized interaction of three different inorganic units (Al, Si, and P) around the surfactant. It leads to uneven columbic interaction among the inorganic units and micellar aggregates of surfactants. Thus, the resultant mesophases suffer the inherent drawback of poor condensation of these units in a T–O–T framework, resulting in structural collapse during calcinations [13]. Traditionally, these mesophases are synthesized via a hydrothermal method in the presence of template consisting of micellar aggregates of long chain surfactants, viz. cetyltrimethylammonium bromide (CTAB) and expensive organic bases, such as TMAOH, TPAOH, and TEAOH. In general, the formation of mesoporous hexagonal aluminophosphates is evident mostly in the presence of alkyl ammonium hydroxide [14]. The formation of mesoporous phase proceeds by weak ion pair interaction between inorganic precursor (I^-) and TMA^+ cation. The poor stability of APO-based material also results if there is strong ion pair interaction between the organic base and inorganic framework [9–12, 14].

Therefore, it is important to have alternative ammonium cations which can generate relatively weak ion pair with the inorganic anionic species and that can be easily removed upon calcination. We believe that the use of

Electronic supplementary material The online version of this article (doi:10.1007/s10853-015-9624-6) contains supplementary material, which is available to authorized users.

✉ Ayyamperumal Sakthivel
sakthiveldu@gmail.com; asakthivel@chemistry.du.ac.in

[1] Department of Chemistry, Inorganic Materials and Catalysis Laboratory, University of Delhi, Delhi 110007, India

ammonium hydroxide instead of alkyl ammonium hydroxide might results in weak ion pair interaction between ammonium cation-inorganic precursors, which may facilitate to diffuse to the surfactant assembly and may favor for ordered mesoporous silicoaluminophosphate (SAPO). In addition, assembling of mesoporous SAPO using a pre-formed microporous precursor unit might enhance structural stability and also show enhanced activity for organic transformations [9–12]. Herein, attempts have been made on the synthesis of mesoporous SAPO assembled from the SAPO-34 precursor in the presence of ammonium hydroxide as the base. Scheme 1 illustrates the synthetic mechanism involved in assembly of mesoporous SAPO-34 from microporous precursors (I^-) in the presence of ammonium cation and surfactant. The resultant mesoporous phase was further stabilized by postsynthetic vapor-phase treatment (VPT) in the presence of tetraethyl orthosilicate (TEOS) and H_2O. The catalytic ability of the resultant material was evaluated for the *trans*-alkylation using naphthalene and 1,3-diisopropylbenzene (DIPB), which is one of the value added process for the utilization of heavier hydrocarbons [15, 16]. The catalytic activity of the stabilized materials was further improved by introducing extra framework Zn (II) ions.

Experimental procedure

Synthesis protocol

The typical synthesis involved three steps. First, the inorganic precursor containing SAPO-34 secondary building units (SBUs) was obtained by a hydrothermal synthetic method with a molar ratio of 1.0 Al_2O_3:1.06 P_2O_5:1.08 SiO_2:2.09 R:66 H_2O (where R is morpholine) as per the previously described procedure [9]. The pre-formed SAPO-34 SBU precursors were, for the first time, assembled into a mesoporous phase using ammonium hydroxide as the base in the presence of CTAB as the surfactant. The assembled mesoporous material with a gel composition of 1.0 Al_2O_3:1.06 P_2O_5:1.08 SiO_2:2.09 R:0.57 CTAB:3.8 NH_4 OH:250 H_2O was subjected to crystallization at 90 °C for 24 h. The resultant as-synthesized material was filtered, dried, and crushed into a fine powder. Subsequently, the as-prepared material is subjected to vapor-phase transformation (VPT) process by placing the finely crushed sample (6 g) in a Teflon cup, which was kept in a Teflon-lined autoclave containing 20 wt% H_2O with 9 mmol of TEOS. VPT was carried on the sample placed in closed environment by steaming at 140 °C for 16 h. Surfactant removal from the as-synthesized and VPT-stabilized materials was accomplished by calcination under atmospheric air at 550 °C for 6 h. The samples prepared with and without the VPT method are represented as M-S-34-N-VPT and M-S-34-N, respectively. About 1–3 wt% of Zn was loaded over M-S-34-N-VPT by incipient wetness method. Prior to introduction of Zn salt [$Zn(NO_3)_2{\cdot}6H_2O$], about 1 gm of M-S-34-N-VPT was dried in air oven at 120 °C for 2 h. Calculated amount of $Zn(NO_3)_2{\cdot}6H_2O$ was dissolved in 2 ml of water and was introduced on M-S-34-N-VPT drop wise. The mixture was stirred for 1 h, dried, and calcined at 550 °C for 6 h.

Characterization

Infra-red spectra were recorded at room temperature on a Perkin-Elmer 2000-FT-IR, in the range 400–4000 cm^{-1} using KBr pellets. Powder X-ray diffraction (XRD) was performed [18 KW XRD Rigaku (2500 V), Japan] with Cu-Kα radiation ($\lambda = 1.5418$ Å) to determine the bulk crystalline phases of the materials. The diffraction patterns were recorded in the 2θ range 0.5°–30°, with a scan speed and step size of 0.5°/min and 0.02°, respectively. The morphology and size of the materials were investigated by scanning electron microscopy [(SEM) EVO/MA15 Zeiss operated at 10–20 kV] and transmission electron microscopy[(TEM), Tecnai G^2 20 S-TWIN

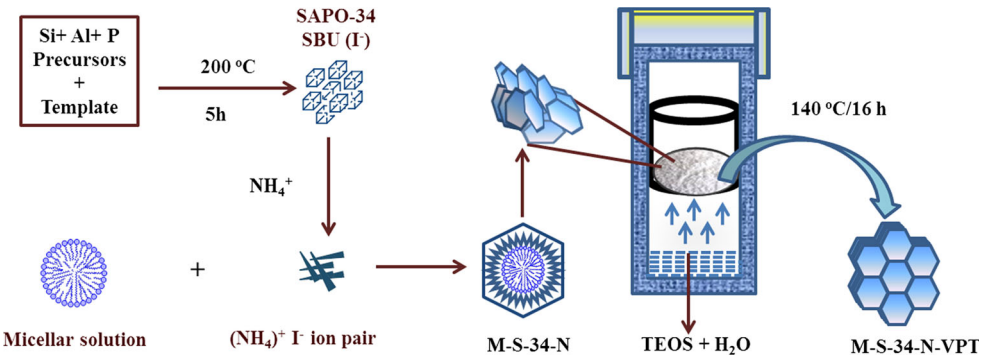

Scheme 1 Pictorial representation of M-S-34-N and M-S-34-N-VPT preparation

operated at 200 kV]. Thermogravimetry (TG) and differential thermal analysis (DTA) measurements of as-synthesized materials were carried out over Perkin-Elmer system in oxygen (200 ml min^{-1}) with a heating rate of 10 °C min^{-1} in the temperature range of 25–900 °C. Nitrogen adsorption/desorption isotherms were recorded on an automatic surface area and porosity analyzer (Micromeritics ASAP 2020, USA). The analysis was carried out at −196°C using samples already degassed at 300 °C for 12–14 h under 0.1333 Pascal pressure. The BET surface area was calculated in the relative pressure range 0.05–0.3, over the adsorption branch of the isotherm. Various other textural properties such as DFT surface area, pore volume (BJH, DFT, HK), and pore size distribution (BJH with Fass correction, calculated over the desorption branch) were elucidated from the isotherm data. Solid-state NMR experiments were carried out on a Bruker AVANCE 400 wide bore spectrometer equipped with a superconducting magnet with a field of 7.1 T using a 4-mm double resonance magic angle spinning (MAS) probe operating at resonating frequencies of 79.4, 104.26, and 161.9 MHz for ^{29}Si, ^{27}Al, and ^{31}P, respectively. The samples were packed in 4-mm zirconia rotors and subjected to a spinning speed of 10 kHz: single pulse experiment with pulse duration of 4.5 μs and a relaxation delay time of 6 s was used for recording all ^{29}Si, ^{27}Al, and ^{31}P MAS NMR patterns. All chemical shift values are expressed with respect to 2,2-dimethyl-2 silapentane-5-sulfonate sodium salt (DSS) for the ^{29}Si nucleus, 85 % H_3PO_4 for the ^{31}P nucleus, and 0.1 M aqueous solution of $Al(NO_3)_3$ for the ^{27}Al nucleus.

Acidity of the samples was followed by pyridine FT-IR spectra collected on a Thermo Scientific Nicolet 6700 FT-IR single-beam spectrometer using a liquid-nitrogen-cooled MCT detector. Pyridine vapor adsorption studies were carried out in a Harrick Scientific HVC-DR2 reaction chamber with a detachable ZnSe window dome, mounted inside a Harrick DRA-2 Praying Mantis diffuse-reflectance accessory designed to minimize parasite specular reflectance. About 100 mg of sample (10 % of material in KBr) was placed in the sample cup and pre-activated at 350 °C for 6 h. For pyridine adsorption, N_2 gas was passed through a pyridine saturator. A partial pressure of 30 mm Hg of pyridine was maintained in the saturator. For pyridine adsorption, the temperature of the sample cup was maintained at 100 °C for 1 h. After pyridine adsorption, the sample was heated to 150 °C and flushed with ultra-high pure N_2 for 1 h to ensure that physically adsorbed pyridine was recovered completely. The sample was cooled to 25 °C and the spectrum was collected using KBr as the background. Further, the sample was degassed at a desired temperature and the spectra were collected.

Catalytic studies

Liquid-phase *trans*-alkylation of naphthalene with C_{12} hydrocarbon, viz. 1,3-DIPB, was studied in an autoclave reactor under stirring condition at autogenous pressure. About 0.1 g of catalyst was added to the reaction mixture containing 1 mmol Naphthalene:20 mmol DIPB mixture. The autoclave was charged to required temperature in an atmosphere of nitrogen for stimulated time. The products were extracted with toluene and analyzed in a HP-5 capillary column (30 m, HP-5) using gas chromatography equipped with flame ionizing detector FID (Agilent 7890A Series). It is important to mention that mono- and di-alkylated products were obtained as major products (see Fig. S1), and only a trace quantity of poly-alkylated naphthalene was evident. Prior to recyclability test, the catalyst was washed with ethanol, dried, and activated at 550 °C for 6 h in air.

Results and discussion

The powder XRD pattern of the materials is presented in Fig. 1. As-synthesized M-S-34-N sample showed a reflection in the 2θ region at 1.2° with a broad pattern around 2.2° corresponding to the (100) and (110) planes of hexagonal mesoporous silicoaluminophosphates [17]. After VPT, the XRD pattern of M-S-34-N-VPT showed well-resolved peaks around 2θ of 1.0° and 1.9°, again corresponding to the (100) and (110) planes of the hexagonal structure. The observed increase in peak intensity and line broadening is due to tethering of uncondensed inorganic

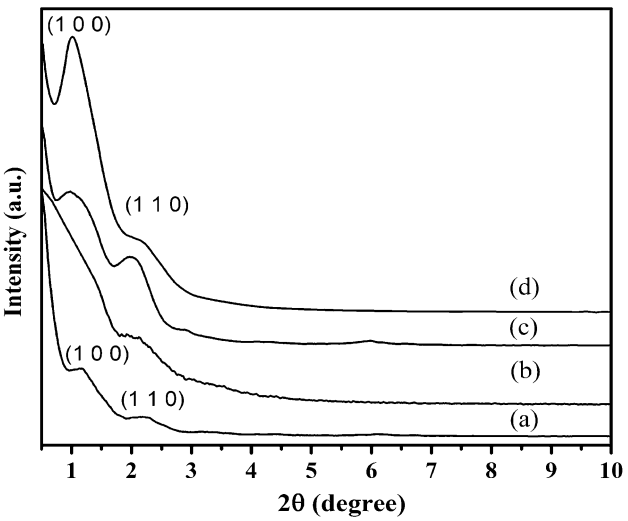

Fig. 1 XRD patterns of as-synthesized M-S-34-N (**a**), calcined M-S-34-N (**b**), as-synthesized M-S-34-N-VPT (**c**) and calcined M-S-34-N-VPT (**d**)

species such as aluminate and phosphate with the help of TEOS on the surface of mesoporous SAPO. Calcination of M-S-34-N before VPT transformation results in weak reflections at 2θ region of 2.1° with a broad hump. Calcined M-S-34-N material showed only weak reflections at 2θ region of 2.1° with a broad hump owing to its short-range order and the inherent uncondensed nature of framework wall, which might partially collapsed upon calcination. However, calcination of sample after VPT (M-S-34-N-VPT) showed well-resolved reflections at 2θ of 1.1° and 2.0°, which are characteristic of the (100) and (110) planes of the hexagonal mesoporous structure. The presence of well-resolved powder XRD reflection peaks for M-S-34-N-VPT indicated the formation of uniform mesoporous materials with long-range order. This structure resulted from the tethering of the partially crystalline framework of aluminate and phosphate species by tetraethylorthosilicate in the presence of steam during VPT. The powder XRD reflection of M-S-N-VPT showed shifts in 2θ toward lower angles. The observed shift is attributed to the expansion of the framework lattice following incorporation of larger tetravalent silicate ions (Si^{4+}, 0.04 nm) at the sites of smaller pentavalent phosphorous ion (P^{5+}, 0.03 nm) in the framework [17, 18]. The well-resolved peaks evident in the postsynthetic steam-stabilized sample (M-S-34-N-VPT) are due to the presence of uniform long-range order in mesoporous SAPO. However, in as-prepared M-S-34-N-VPT, the broad X-ray reflections correspond to the incorporation of silicate species along with the presence of occluded surfactants in mesoporous channels. It is expected that in as-VPT-treated sample, the TEOS introduced during VPT processes is mostly present on uncondensed framework sites of mesopore. As the calcination proceeds, the uncondensed sites are tethered by these Si units, finally giving a well-ordered mesoporous M-S-34-N-VPT, with well-resolved XRD reflections and high intensity.

The FT-IR spectrum (shown in Fig. 2) of the M-S-34-N sample shows vibrational bands at 730 and 1096 cm^{-1}, ascribed to the symmetric and asymmetric stretching frequencies of the T–O–T species (where T = Si, Al, and P). The additional strong band observed around 635 cm^{-1} arises from the T–O–T bending vibrations of the D6R SBUs of the microporous SAPO-34 framework [9, 19–21]. The presence of secondary building unit (SBU) was evident even after VPT process (Fig. 2), thus indicating that the microporous unit retains on the wall of mesoporous SAPO-34. The introduction of zinc shows additional band around 914 cm^{-1}, a characteristic of Si–O–M stretching band. The N_2 sorption isotherms of M-S-34-N and M-S-34-N-VPT are depicted in Fig. 3. Both the samples exhibit the presence of type I and type IV isotherms [9, 22–24]. The type I isotherm evident at relative pressures (p/p_0) of 0.1

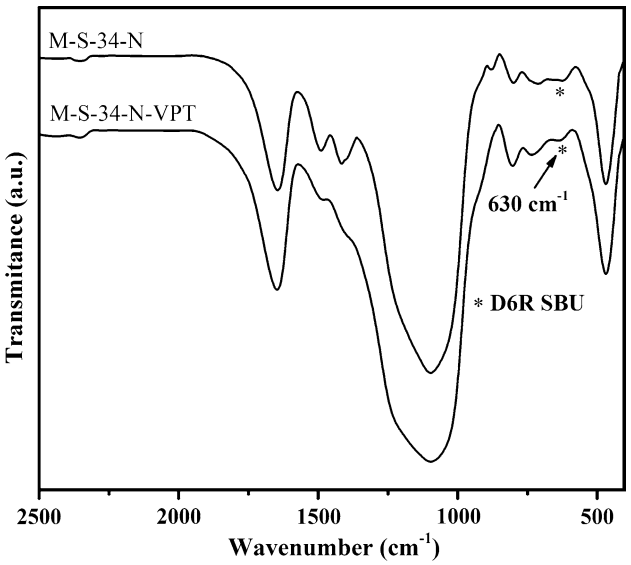

Fig. 2 FT-IR spectra of as-synthesized M-S-34-N (**a**), M-S-34-N-VPT (**b**)

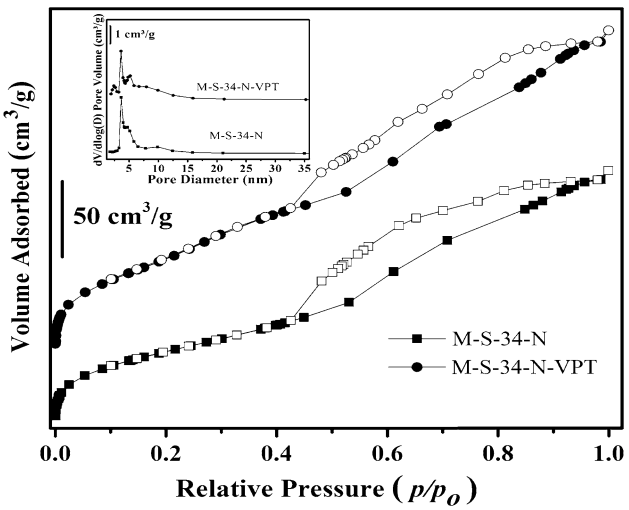

Fig. 3 N_2 sorption isotherm of mesoporous silicoaluminophosphate of before and after VPT treatment; *inset* shows pore size distribution of corresponding samples

corresponds to the microporous SBU precursor unit present on the mesopore walls. The distinct type IV isotherm also evident with the increase in adsorption in the region of p/p_0 between 0.4 and 0.9 is due to capillary condensation in the mesopore [22–24]. The key difference between the M-S-34-N and M-S-34-N-VPT isotherms is a steep increase in the adsorption quantity in the mesopore region of M-S-34-N-VPT owing to the formation of a uniform mesopore channel after VPT. The isotherms are associated with a combination of H2 and H3 hysteresis loops, which are attributed to the presence of interconnected pores with "ink-bottle" type geometry and slit-shaped pores owing to

aggregates of plate-like particles, respectively [9, 12, 23]. The effect of vapor-phase treatment is clearly evident in the textural properties summarized in Table 1. M-S-34-N had a BET surface area and pore volume of 444 m^2 g^{-1} and 0.6 cm^3 g^{-1}, respectively. The significant increase in these properties after VPT to 621 m^2 g^{-1} and 0.8 cm^3 g^{-1}, respectively, clearly supports the formation of uniform mesoporosity in M-S-34-N-VPT. The TEM image of M-S-34-N-VPT (Fig. 4) clearly shows hierarchical pore with the dimensions of around 4.0 nm, which agrees well with the BJH pore diameter (Fig. 3 inset) evident from the N_2 sorption analysis. The SEM analysis revealed that M-S-34-N-VPT (Fig. 5) is composed of elongated hexagonal plates with particles sizes of 5–8 μm. The presence of hexagonal plate-like particles lies in well accordance with H3 hysteresis loop observed in N_2 sorption isotherm. The TG/DTA analysis of as-synthesized M-S-34-N-VPT (Fig. 6) exhibited three weight loss stages (total 46 wt%), with respective endothermic transitions. The first endothermic weight loss below 150 °C (5 wt%) is assigned to the desorption of physisorbed water. The major weight loss from 150–350 °C (30 wt%) and above (11 wt%) is due to decomposition of CTAB and water loss from the condensation of surface hydroxyl groups present in the framework [9]. The local coordination environment of the Al and Si atoms was studied by ^{27}Al and ^{29}Si MAS NMR. The ^{27}Al MAS NMR spectrum of M-S-34-N-VPT, shown in Fig. 7, has prominent signals centered at −5.9 and 43.6 ppm with a weak shoulder at 9.4 ppm corresponding to hexa-coordinated $[Al(OP)_x(OH)_{6-x}]$, tetra-coordinated $[Al(OP)_4]$, and penta-coordinated $[Al(OP)_x(OH)_{5-x}]$ species, respectively [25–28]. The degree of condensation of silica in the SAPO framework was studied by ^{29}Si MAS NMR. The as-synthesized sample (Fig. 8) shows three peaks centered around −108, −102, and −90 ppm representing Q^4 [Si(0Al)], Q^2 [Si(2Al)], and Q^1 [Si(3Al)] sites. Direct calcination of mesoporous SAPO (M-S-34-N) resulted in an increase in intensity of the Q^2 and Q^1 sites owing to uncondensed silicate species. In addition, a new peak centered at −94 ppm, corresponding to tetra-coordinated $Si(OAl)_4$ species. It suggests that a few Si species gets incorporated in tetrahedral framework by direct calcinations. On the other hand, calcination of mesoporous SAPO after VPT (M-S-34-N-VPT) yielded enhanced signal intensities for the Q^4 and Q^2 sites, which clearly supports that VPT helps to tether uncondensed species and favors the formation of uniform mesoporous channel [29–31]. Further, the presence of more Q^3 and Q^4 signals (around −100 ppm) unlike conventional SAPO molecular sieve materials resulted due to incorporation of silica during the tethering process [17]. The acidity of the M-S-34-N-VPT sample was determined by following pyridine desorption in FT-IR spectra, as depicted in Fig. 9. The sample exhibited vibrational bands with strong intensities around 1440–1450 cm^{-1} corresponding to pyridine bound to Lewis acid sites. These bands were retained at high desorption temperatures (550 °C), indicating the presence of strong Lewis acid sites [6, 11]. The characteristic bands of Brönsted acid sites are relatively less intense and were decreased by the increase in desorption temperature. This result suggests that the Brönsted acid sites on the surface of M-S-34-N-VPT are moderate in nature [9]. The well-characterized hierarchical mesoporous SAPO material, viz. M-S-34-N-VPT, was evaluated for *trans*-alkylation of naphthalene with 1,3-DIPB in a liquid-phase medium (Table 2). It is worth mention here that alkylated naphthalene is an important raw material for the fabrication of polyester [32]. Conventionally alkyl naphthalenes are obtained by Friedel-Craft alkylation of naphthalene using various alkylating agents in the presence of strong acids. We have attempted to prepare value-added heavier hydrocarbons by *trans*-alkylation of naphthalene using solid acid catalyst.

In order to achieve better conversion, reaction parameters such as effect of temperature, molar ratio of substrates employed in the reaction, were systematically evaluated. The reaction does not proceed in the absence of catalyst. The effect of temperature on *trans*-alkylation over M-S-34-N-VPT was evaluated in the range of 160–225 °C for 12 h, and the results are shown in Fig. S2. The results depict that at lower temperature, viz. 160 °C, only around 10 % conversion was obtained. The conversion steadily increases with increase in temperature and reaches to maximum of about 18 % at 200 °C. With further increase in temperature, there is no appreciable change in conversion owing to the reversible nature of the reaction. Hence, further studies were carried out by keeping the temperature at 200 °C for 12 h. The effect of substrates molar ratio (naphthalene:1,3-DIPB) was studied from 1:5 to 1:20, and the results are shown in Table 2. It reveals that when naphthalene ratio is higher (1:5–1:10), only 7–8 % conversion was obtained. The use of less DIPB results in competitive interaction of

Table 1 Textural properties of M-S-34-N and M-S-34-N–VPT materials

Samples	Surface area (m^2/g)		BJH pore volume (cm^3/g)	Average pore diameter (nm)
	BET	DFT		
M-S-34-N	444	669	0.6	4.6
M-S-34-N-VPT	621	873	0.7	4.4

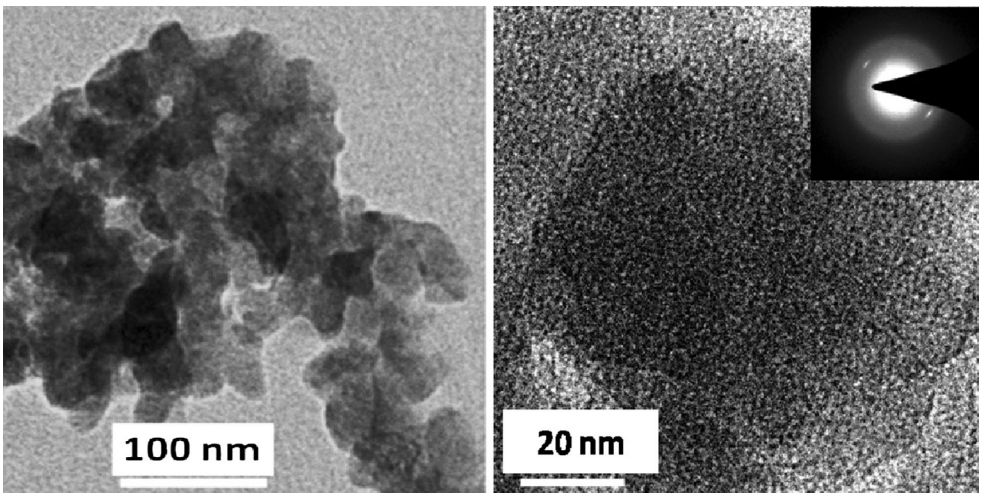

Fig. 4 TEM images of M-S-34-N-VPT

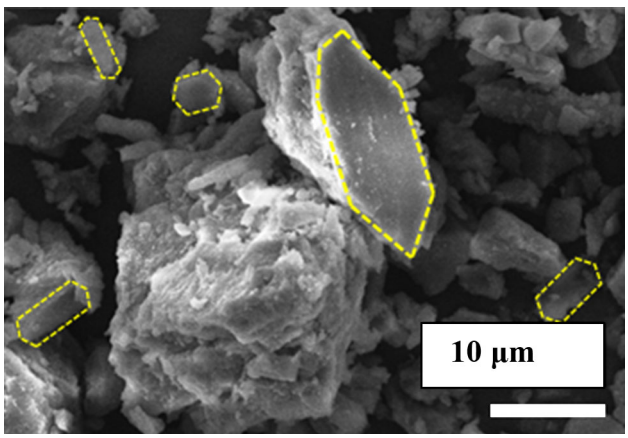

Fig. 5 SEM images of M-S-34-N-VPT sample

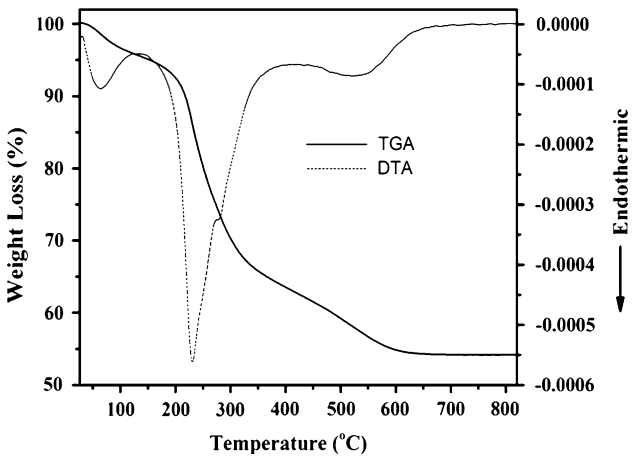

Fig. 6 TG-DTA profile of as-synthesized M-S-34-N-VPT

naphthalene along with DIPB on active sites and thus results in low conversion. With increase in the molar ratio (1:15), an increase in the conversion of around 11 % was

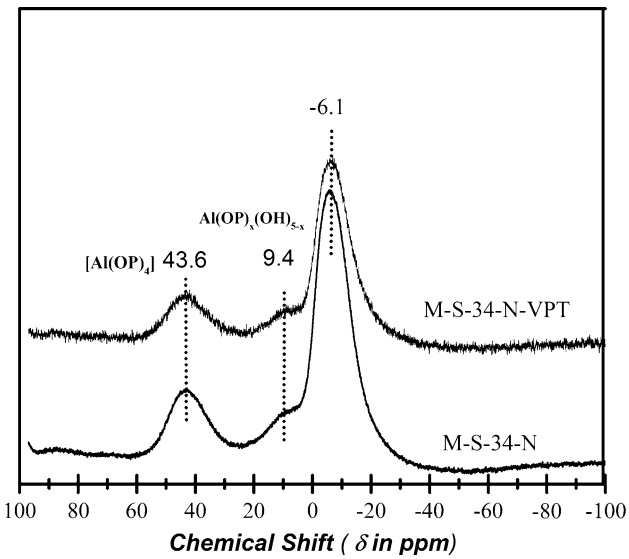

Fig. 7 ^{27}Al MAS NMR spectra of M-S-34-N and M-S-34-N-VPT samples

obtained, while maximum conversion of more than 18 % was evident when substrate molar ratio was 1:20. This is attributed to the homogenous distribution of solid naphthalene in the DIPB phase, which offers the better accessibility of the reactant molecules to the active sites of catalyst. Further increase in substrates molar ratio does not appreciably alter the yield. Finally, reactions were carried out under discussed optimized condition using different catalysts, and the results are shown in Table 3. Microporous SAPO-34 showed only 1.2 % conversion owing to its small pore openings. The small pore opening of SAPO-34 (0.34 nm) restricts the diffusion of bulkier poly-alkylatednaphthalene molecules (0.66–1 nm) [33, 34] which results in high selectivity for 1-isopropyl naphthalene.

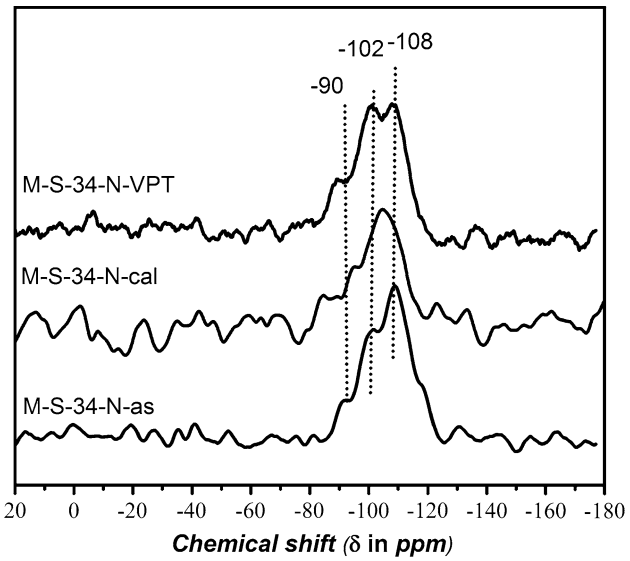

Fig. 8 ^{29}Si MAS NMR spectra of various mesoporous SAPO samples

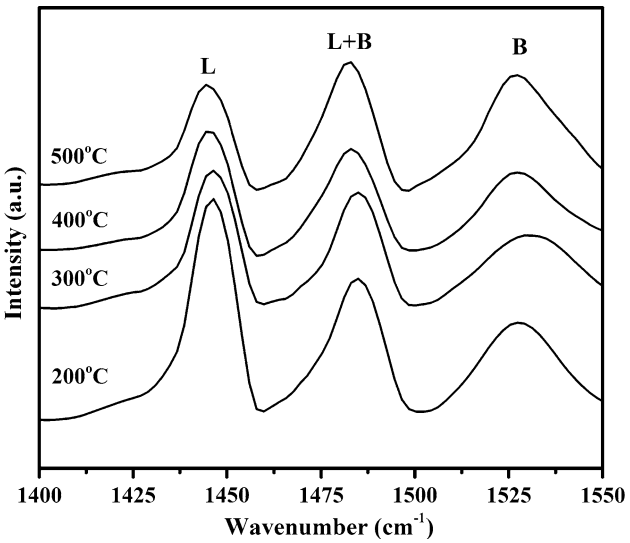

Fig. 9 FT-IR pyridine desorption spectra of M-S-34-N-VPT

Table 3 *Trans*-alkylation of naphthalene using 1,3-DIPB

Catalysts	Conv. (%)	Selectivity (%)[a]		
		1-IPN	2-IPN	Di-IPN
M-S-34-N-VPT	18.3	30.4	45.5	24.2
1st recycle	20.2	23.6	53.2	23.2
2nd recycle	19.2	23.5	55.5	21
M-S-34-N	10.7	24.5	52.4	14.1
SAPO-34	1.2	67.3	31.4	2.3
No catalyst	0.0	–	–	–

Reaction conditions: catalyst = 100 mg, Temperature = 200 °C, duration = 12 h, naphthalene and DIPB molar ratio (1:20)

[a] Iso-propyl naphthalene

M-S-34-N showed a conversion of 10.7 % with about 77 % selectivity for mono-isopropyl naphthalene as the major product. The use of M-S-34-N-VPT enhanced the catalytic conversion to about ~18 % with similar product selectivity. The observed higher conversion using M-S-34-N-VPT compared with M-S-34-N is a result of the long-range order and strong Lewis acidity present on the M-S-34-N-VPT surface. Importantly, the catalytic conversion remains almost the same, even after the second recycle. It is known from the literature that introduction of Lewis acidic metals (Zn and Fe) nearby Brönsted acidic sites facilitates a synergic effect between neighboring Brönsted and Lewis acidic sites, which enhance the catalytic activity of alkylation reactions [35–38]. The chosen reaction in the present study is an example of electrophilic aromatic substitution where Lewis acidity of the catalyst plays a vital role [35–38]. Thus, in order to improve the catalytic conversion, M-S-34-N-VPT was modified with Zn and Fe (1.5 wt%) by incipient wetness method. The catalytic results on Fe- and Zn-loaded M-S-34-N-VPT are summarized in Table 4. The introduction of Fe and Zn enhances the catalytic conversion of naphthalene to 27 and 31 wt%, respectively. The above fact might be due to the increase in surface acidity

Table 2 Effect of reactant's molar ratio (naphthalene:1,3-DIPB) on *trans*-alkylation of aromatics over M-S-34-N-VPT

S. no	Naphthalene:DIPB	Conversion (%)	Selectivity (%)[a]		
			1-IPN	2-IPN	Di-IPN
1	1:5	6.7	21.3	57.5	21.2
2	1:10	8.3	23.6	57.9	18.5
3	1:15	10.6	27.9	49.7	22.4
4	1:20	18.3	30.4	45.5	24.2

Reaction conditions: catalyst = 100 mg, temperature = 200 °C, duration = 12 h

[a] Iso-propyl naphthalene

Table 4 Effect of metal loading on M-S-34-N-VPT over *trans*-alkylation of aromatics

Metal loading (wt%)	Conv. (%)	Selectivity (%)[a]			
		1-IPN	2-IPN	Di-IPN	Tri-IPN
0.0	18.3	30.4	45.5	24.2	–
1.5 Zn	30.8	40.3	10.4	37.7	11.6
1.5 Fe	26.9	32.1	19.6	28.1	20.2

Reaction conditions: catalyst = 100 mg, Temperature = 200 °C, duration = 12 h, naphthalene and DIPB molar ratio (1:20)

[a] Iso-propyl naphthalene

upon introduction of Fe and Zn [39], which facilitates improvement in conversion. Further, the selectivity toward di-alkylated and poly-alkylated (tri-alkylated) naphthalene increases with the cost of mono-isopropylated naphthalene owing to the enhance in surface acidity with the introduction of Fe and Zn. The extra framework metal sites facilitate the formation of isopropyl carbenium ion and favored the observed higher conversion. Further, it is interesting to note that the observed *trans*-alkylation activity on Zn-loaded M-S-34-VPT samples showed even better than strongly acidic nanosize ZSM-5 catalyst (29 %).

Conclusion

Hierarchical, stable mesoporous SAPO was synthesized using ammonium hydroxide as the base with the help of microporous SAPO-34 precursors. Furthermore, the obtained material was stabilized using VPT. The VPT method helped in tethering of uncondensed inorganic species to the crystallized mesophase. The resultant material possessed a uniform mesoporous channel with good surface area and pore volume, as well as strong Lewis acidity, which makes the material suitable for *trans*-alkylation of alkylbenzenes. The introduction of zinc on the external surface of M-S-N-VPT enhances surface acidity which improves the catalytic conversion and the poly-alkylated naphthalene products selectivity.

Acknowledgements The authors are grateful to DST (SR/S1/PC-11/2011) and UGC [no. 41-237/2012/(SR)] India, for the financial support. The authors also express their sincere thanks to USIC, University of Delhi, and CSIR-CECRI Karaikudi, for their support on instrumentation facility. AKS and RY are grateful to CSIR and UGC, India, for their SRF.

References

1. Sun Q, Wang N, Xi D, Yang M, Yu J (2014) Organosilane surfactant-directed synthesis of hierarchical porous SAPO-34 catalysts with excellent MTO performance. Chem Commun 50:6502–6505
2. Moliner M, Martínez C, Corma A (2014) Synthesis strategies for preparing useful small pore zeolites and zeo-types for gas separations and catalysis. Chem Mater 26:246–258
3. Hamoudi S, Belkacemi K (2013) Adsorption of nitrate and phosphate ions from aqueous solutions using organically-functionalized silica materials: kinetic modeling. Fuel 110:107–113
4. Sakthivel A, Huang SJ, Chen WH, Lan ZH, Chen KH, Lin HP, Mou CY, Liu SB (2005) Direct synthesis of highly stable mesoporous molecular sieves containing zeolite building units. Adv Funct Mater 15:253–258
5. Calleja G, Aguado J, Carrero A, Moreno J (2005) Chromium supported onto swelled Al-MCM-41 materials: a promising catalysts family for ethylene polymerization. Catal Commun 6:153–157
6. Poyraz AB, Dag O (2009) Role of organic and inorganic additives on the assembly of CTAB-P123 and the morphology of mesoporous silica particles. J Phys Chem C 113:18596–18607
7. Sakthivel A, Huang SJ, Chen WH, Lan ZH, Chen KH, Kim TW, Ryoo R, Chiang AST, Liu SB (2004) Replication of mesoporous aluminosilicate molecular sieves (RMMs) with zeolite framework from mesoporous carbons (CMKs). Chem Mater 16:3168–3175
8. Sakthivel A, Komura K, Sugi Y (2008) MCM-48 supported tungstophosphoric acid: an efficient catalyst for the esterification of long-chain fatty acids and alcohols in supercritical carbon dioxide. Ind Eng Chem Res 47:2538–2544
9. Singh AK, Yadav R, Sakthivel A (2013) Synthesis, characterization, and catalytic application of mesoporous SAPO-34 (MESO-SAPO-34) molecular sieves. Microporous Mesoporous Mater 181:166–174
10. Yadav R, Singh AK, Sakthivel A (2013) Unique mesoporous silicoaluminophosphate assembled from faujasite-type SAPO-37 precursor: a potential catalyst for isomerization. Chem Lett 42:1160–1162
11. Yadav R, Singh AK, Sakthivel A (2015) Mesoporous silicoaluminophosphates derived from microporous precursors as promising catalyst for hydroisomerization. Catal Today 245:155–162
12. Singh AK, Yadav R, Sudarsan V, Kishore K, Upadhyayula S (2014) Sakthivel a mesoporous SAPO-5 (MESO-SAPO-5): a potential catalyst for hydroisomerisation of 1-octene. RSC Adv 4:8727–8734
13. Kimura T (2005) Surfactant-templated mesoporous aluminophosphate-based materials and the recent progress. Microporous Mesoporous Mater 77:97–107
14. Zaho D, Luon Z, Kevan L (1997) Synthesis of thermally stable mesoporous hexagonal aluminophosphate molecular sieves. Chem Commun 11:1009–1010
15. Nesterenko NS, Kuznetsov AS, Timoshin SE, Fajula F, Ivanova II (2006) *Trans*-alkylation of polynuclear aromatics with diisopropylbenzene over zeolite catalysts. Appl Catal A 307:70–77

16. Kamalakar G, Kulkarni SJ, Raghavan KV, Unnikrishnan S, Halgeri AB (1999) Isopropylation of naphthalene over modified HMCM-41, HY and SAPO-5 catalysts. J Mol Catal A 149:283–288
17. Singh AK, Kishore K, Yadav R, Upadhyayula S, Sakthivel A (2014) Uniform mesoporous silicoaluminophosphate derived by vapor phase treatment: its catalytic and kinetic studies in hydroisomerization of 1-Octene. J Phys Chem C 118:27961–27972
18. Shannon RD, Prewitt CT (1969) Effective ionic radii in oxides and fluorides. Acta Cryst B 25:925–946
19. Tan J, Liu Z, Bao X, Liu X, Han X, He C, Zhai R (2002) Crystallization and Si incorporation mechanisms of SAPO-34. Microporous Mesoporous Mater 53:97–108
20. Liu G, TianP Li J, Zhang D, Zhou F, Liu Z (2008) Synthesis, characterization and catalytic properties of SAPO-34 synthesized using diethylamine as a template. Microporous Mesoporous Mater 111:143–149
21. Prakash AM, Unnikrishnan S (1994) Synthesis of SAPO-34: high silicon incorporation in the presence of morpholine as template. J Chem Soc Faraday Trans 90:2291–2296
22. Kruck M, Jaroniec M (2001) Gas adsorption characterization of ordered organic-inorganic nanocomposite materials. Chem Mater 13:3169–3183
23. Sing KSW, Everett DH, Haul RAW, Moscou L, Pierotti RA, Rouquerol T, Siemienewska T (1985) Reporting physisorption data for gas/solid systems with special reference to the determination of surface area and porosity. Pure Appl Chem 57:603–619
24. Choi M, Srivastava R, Ryoo R (2006) Organosilane surfactant-directed synthesis of mesoporous aluminophosphates constructed with crystalline microporous frameworks. Chem Commun 42:4380–4382
25. Kimura T, Sugahara Y, Kuroda K (1998) Synthesis of mesoporous aluminophosphates and their adsorption properties. Microporous Mesoporous Mater 22:115–126
26. Zhao XS, Lu GQM (2001) Aluminophosphates-based mesoporous molecular sieves: synthesis and characterization of TAPOS. Microporous Mesoporous Mater 44–45:185–194
27. Campelo JM, Jaraba M, Luna D, Luque R, Marinas JM, Romero AA, Navio JA, Macias M (2003) Effect of phosphate precursor and organic additives on the structural and catalytic properties of amorphous mesoporous $AlPO_4$ materials. Chem Mater 15:3352–3364
28. Feng P, Xia Y, Feng J, Bu X, Stucky GD (1997) Synthesis and characterization of mesostructured aluminophosphates using the fluoride route. Chem Commun 10:949–950
29. Zhao GL, Zhang XJ, Chen TH, Yuan ZY (2006) Synthesis of mesoporous aluminophosphate and silicoaluminophosphate in the presence of nonionic poly(ethylene oxide) surfactant. Mater Sci Eng B 131:263–266
30. Shen W, Li X, Wei Y, Tian P, Deng F, Han X, Bao X (2012) A study of the acidity of SAPO-34 by solid-state NMR spectroscopy. Microporous Mesoporous Mater 158:19–25
31. Shin HS, Hwang YK, Huh S (2014) Facile preparation of ultra-large pore mesoporous silica nanoparticles and their application to the encapsulation of large guest molecules. Appl Mater Interfaces 6:1740–1746
32. Shiroto Y, Shimura M, Shimokawa K, Fukui Y, Asaoka S, Tajima H, Ueda K, Tachibana Y, Tate K, Taniguchi H, Kuki (1990), Process for the Production of 2,6-Diisopropylnapthalene US Patent 4,950,824
33. Tasi G, Mizukami F, Palinko I, Toba M, Kukovecz A (2001) Positional isomerization of dialkylnaphthalenes: a comprehensive interpretation of the selective formation of 2,6-DIPN over HM zeolite. J Phys Chem A 105:6513–6518
34. Brzozowski R, Vinu A, Mori T (2007) Alkylation of naphthalene using propylene over mesoporous Al-MCM-48 catalysts. Catal Commun 8:1681–1683
35. Corma A, García H (1997) Organic reactions catalyzed over solid acids. Catal Today 38:257–308
36. Narayanan S, Deshpande K (2000) Aniline alkylation over solid acid catalysts. Appl Catal A 199:1–31
37. Pivsa-Art S, Okuro K, Miura M, Murata S, Nomura M (1994) Acylation of 2-methoxynaphthalene with acyl chlorides in the presence of a catalytic amount of lewis acids. J Chem Soc Perkin Trans 1:1703–1707
38. Savidha R, Pandurangan A, Palanichamy M, Murugesan V (2004) A comparative study on the catalytic activity of Zn and Fe containing Al-MCM-41 molecular sieves on t-butylation of phenol. J Mol Catal A 211:165–177
39. Banu M, Lee YH, Magesh G, Lee JS (2014) Isopropylation of naphthalene by isopropanol over conventional and Zn- and Fe-modified USY zeolites. Catal Sci Tech 4:120–128